Supplementary information

Cobalt Vacancies Assisted Ions Diffusion in Co_2AlO_4/Carbon Nanofibers for Enhancing Lithium Battery Performance

Qian Shi, Yin Zhang, Kaiyun Chen, Shuang Yuan, Fanghua Tian, Tieyan Chang, Yangqin Cheng, Kangkang Yao, Sen Yang and Xuan Zhou**

SEM and TEM images of Co_2AlO_4/C NFs and Co_2AlO_4 NFs: By observing the SEM images of Co_2AlO_4/C NFs and Co_2AlO_4 NFs through Fig. S1a and Fig. S1b, they are all continuous nanofibers with different diameters. Many Co_2AlO_4 nanoparticles embedded in carbon nanofibers were observed by the TEM image in Fig. S1c. The HRTEM image shows the excellent graphitization of carbon nanofibers with an interplanar spacing of 0.33 nm corresponding to (002) surface and the nanoparticles are encased in graphite with interplanar spacing of 0.28 nm and 0.24 nm corresponding (220) and (311) surface of Co_2AlO_4 in Fig. S1e. Nanofibers are composed of Co_2AlO_4 nanoparticles shown in Fig. S1d. The HRTEM image shows regular crystal faces of 0.47nm and 0.28nm correspond to (111) and (220) surface of Co_2AlO_4 in Fig. S1f.

Composition ratio in Co_2AlO_4/C NFs @ Co_2AlO_4 NS and Co_2AlO_4/C NFs respectively: To clearly investigate the degree of graphitization and the thermal behavior of carbon in Co_2AlO_4/C NFs @ Co_2AlO_4 NS. The Raman spectrum of the material is shown in the Fig. S2a. The spectrum of Co_2AlO_4/C NFs @ Co_2AlO_4 NS composites clearly exhibited a pair of peaks at 1323.8 and 1597.5 cm^{-1}, corresponding to a defect or disorder evoked D band and a crystalline G band of graphitic materials, respectively. The large intensity of D band implied that there are numerous sp3 structures in the carbon nanofibers, which were probably introduced during calcinations. These amorphous carbons should partially decompose less than 300°C, which has been reported in previous works[1-2]. The proportion of carbon and Co_2AlO_4 in Co_2AlO_4/C NFs

@ Co_2AlO_4 NS and Co_2AlO_4/C NFs can be understood in Fig. S2b, which ~30% carbon and ~70% Co_2AlO_4 are in Co_2AlO_4/C NFs @ Co_2AlO_4 NS and ~34% carbon and ~66% Co_2AlO_4 are in Co_2AlO_4/C NFs.

Rate performance of Co_2AlO_4/C NFs: The Co_2AlO_4/C NFs electrode shows poor cyclic stability at a current density of 100mA g^{-1}. The specific discharge capacity of Co_2AlO_4/C NFs only remains at 482.3 mAh g^{-1} after 10 cycles. The rate performance of the Co_2AlO_4/C NFs electrode is much lower than Co_2AlO_4/C NFs @ Co_2AlO_4 NS electrode.

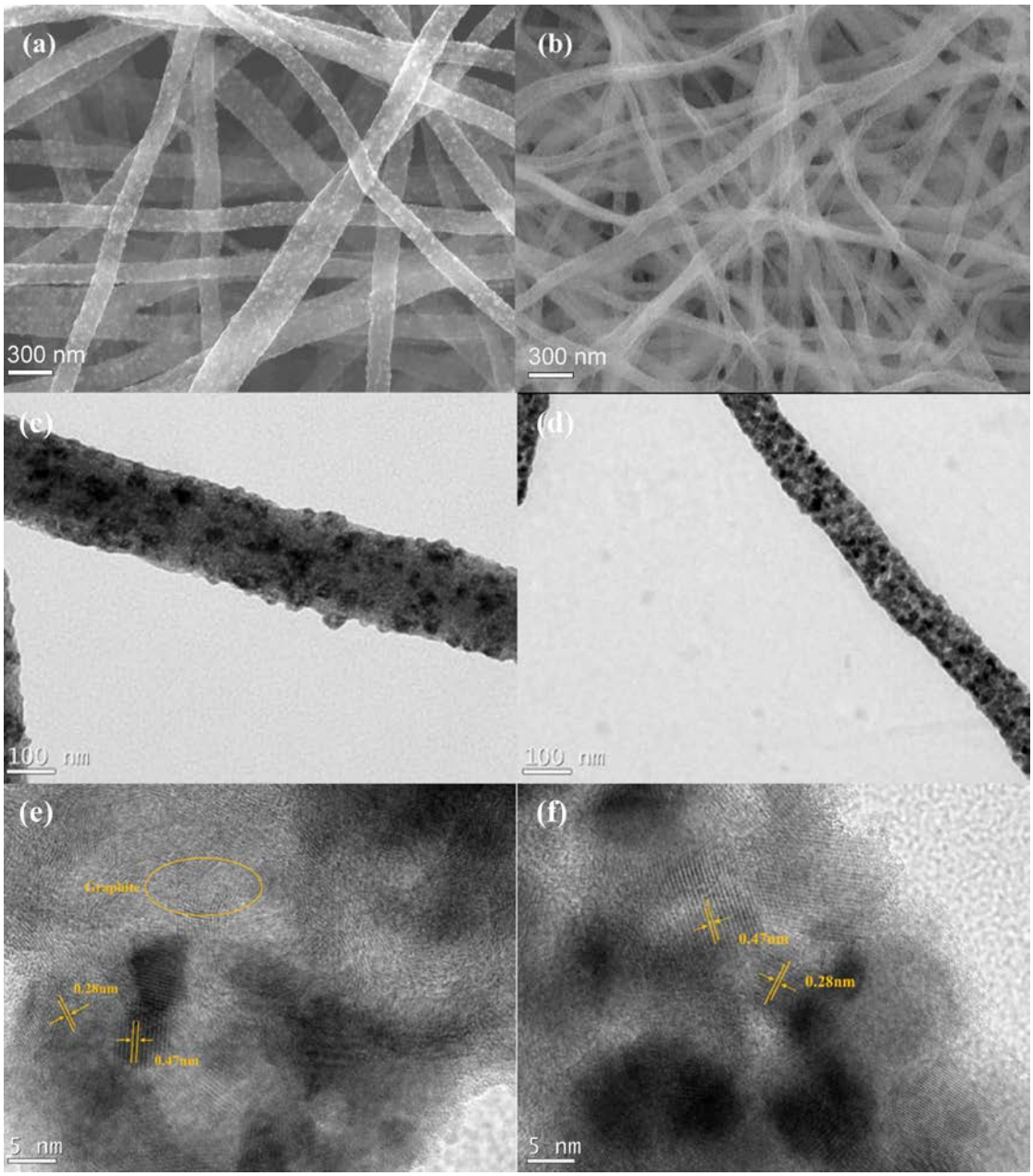

Fig. S1. SEM images of (a) Co_2AlO_4/C NFs and (b) Co_2AlO_4 NFs, TEM images of (c)Co_2AlO_4/C NFs and (d) Co_2AlO_4 NFs, HRTEM images of (e) Co_2AlO_4/C NFs and (f)Co_2AlO_4 NFs

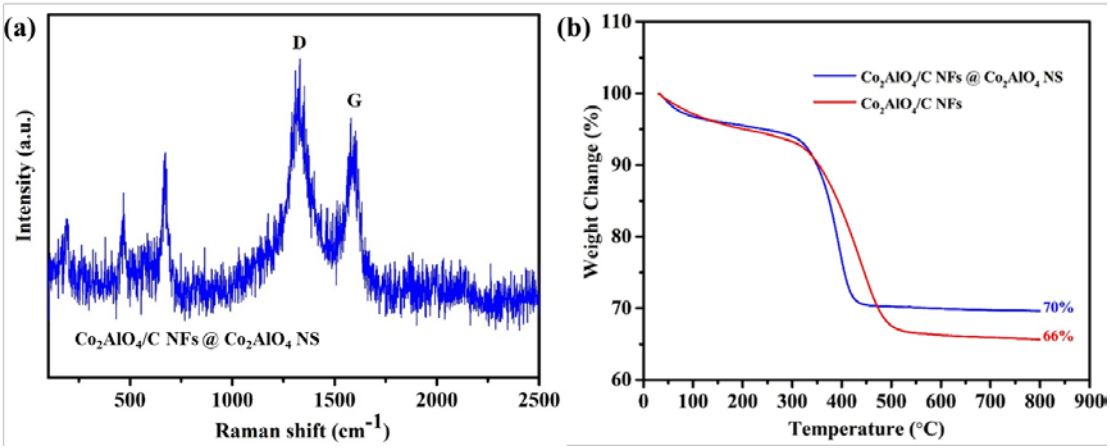

Fig. S2. (a) Raman spectrum of Co_2AlO_4/C NFs @ Co_2AlO_4 NS, (a) TGA curves of different samples.

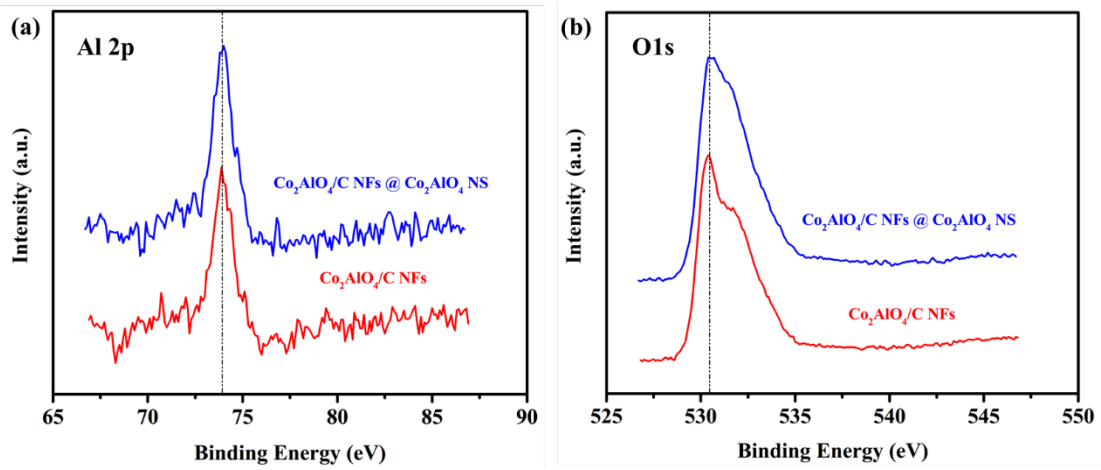

Fig. S3. High resolution XPS spectra of the (a) O1s, (b) Al 2p of Co_2AlO_4/C NFs @ Co_2AlO_4 NS and Co_2AlO_4/C NFs.

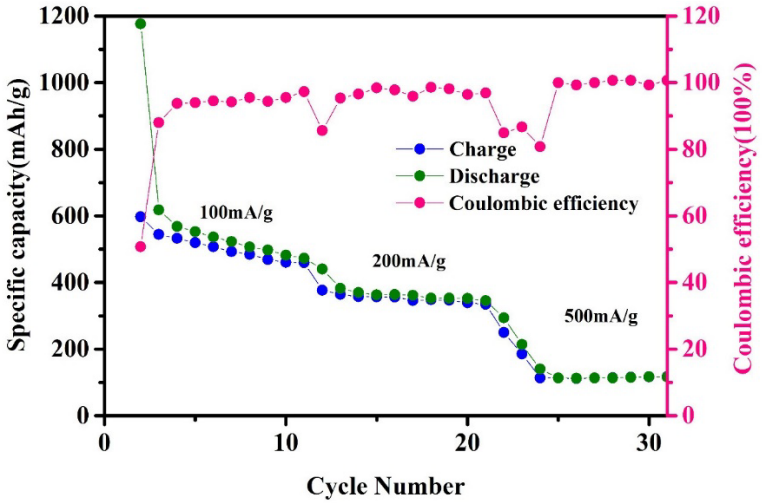

Fig. S4. Rate performance of Co_2AlO_4/C NFs at various current density.

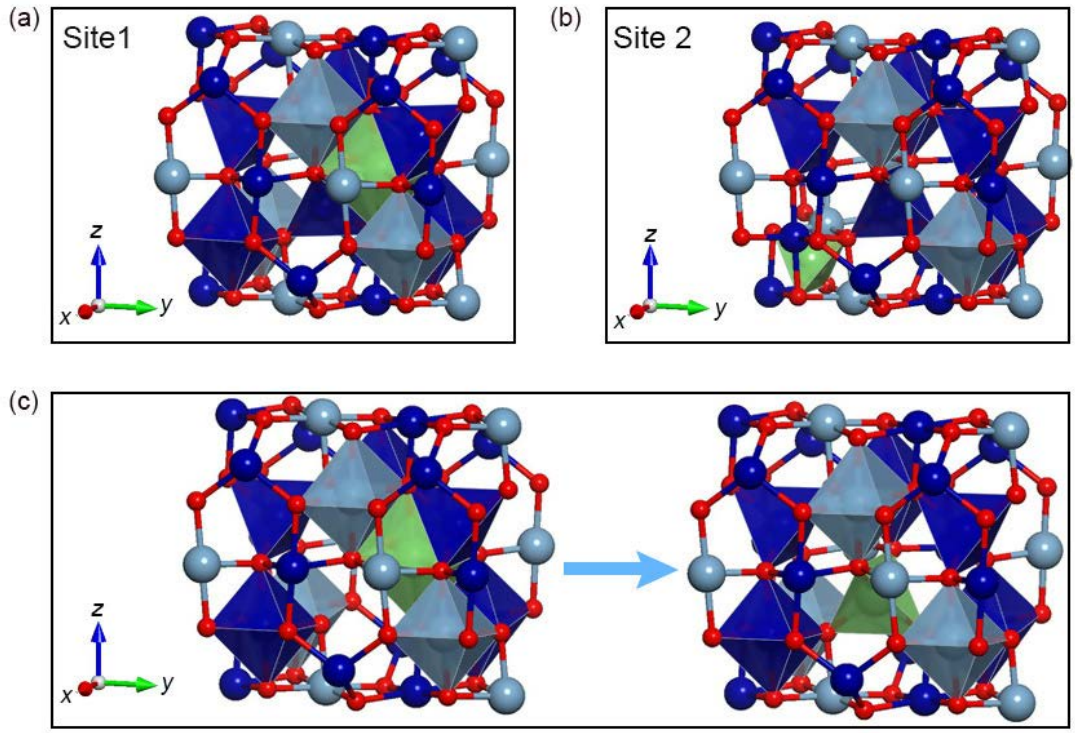

Fig. S5. Li distribution site. (a) site 1 for Li atom distribution without Co vacancy. (b) site 2 for Li atom distribution without Co vacancy. (c) Li at site 1 will spontaneously migrate to the vacancy site once Co vacancy forms.

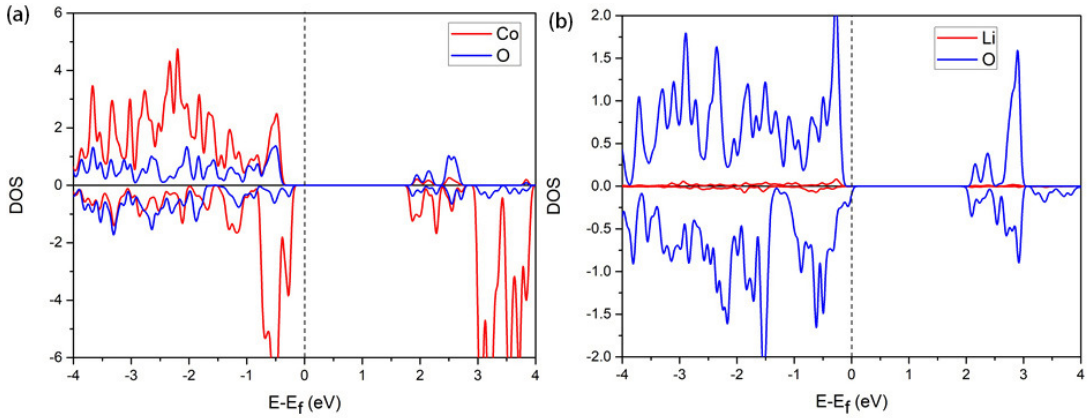

Fig. S6. Density of state (DOS) of Co, Li and O atoms. (a) DOS of Co and O atom in Co_2AlO_4 without vacancy. (b) DOS of Li and O atom in Co_2AlO_4 with Co at the tetrahedral site being replaced by Li. From DOS, it can be seen that the bonds between Co and O are stronger than those between Li and O. It means that once Co at the tetrahedral site is located by Li atoms, Li atom is much easy displacement during Li migration process between tetrahedral interstice, explaining the energy barrier decrease.

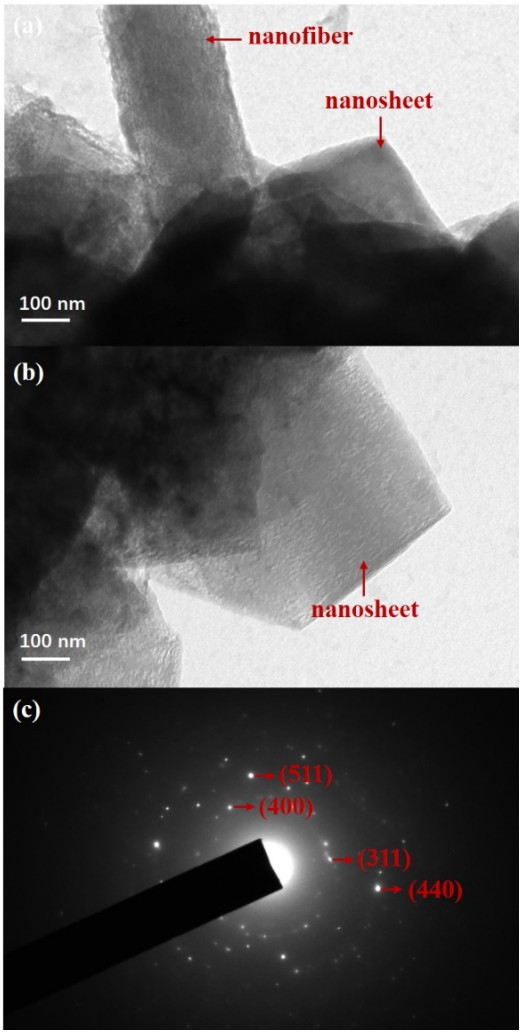

Fig. S7. (a) and (b) are TEM images at different region, and (c) is SAED pattern of Co_2AlO_4/C NFs @ Co_2AlO_4 NS at a current density of 500 mA g^{-1} after 500 cycles.

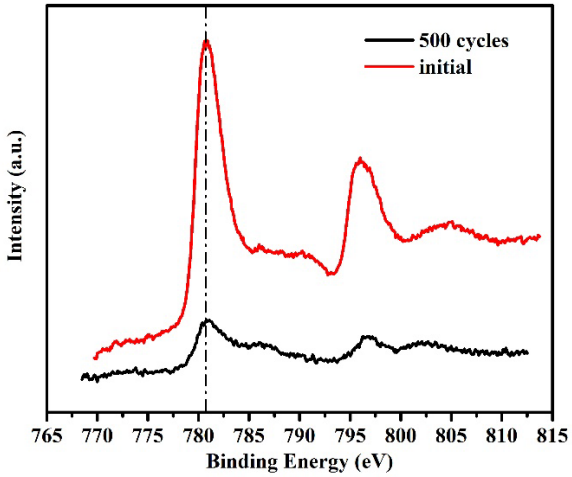

Fig. S8. High-resolution XPS spectra of the Co 2p of Co_2AlO_4/C NFs @ Co_2AlO_4 NS in initial state and after 500cycles.

Table S1
Summary of the electrochemical performance of various anode materials with similar morphologies.

Active substance	**Cyclic stability**	**Refs**
MoS_2 nanoplates embedded in Carbon nanofibers	after 100 cycles, 1007 $mAhg^{-1}$ at 100mAg^{-1}	[3]
SnO_2 nanoflowers on N-doped carbon nanofibers	after 100 cycles, 750 $mAhg^{-1}$ at 100mAg^{-1}	[4]
carbonaceous backbones supported $MoSe_2$ nanosheets	after 100 cycles, 610.8 $mAhg^{-1}$ at 100mAg^{-1}	[5]
Porous carbon nanofiber @MoS_2 core/sheath fiber	after 50 cycles, 736 $mAhg^{-1}$ at 50mAg^{-1}	[6]
N-doped carbon encapsulated FeS nanosheets with amorphous TiO_2	after 500 cycles, 402.5 $mAhg^{-1}$ at 1000mAg^{-1}	[7]
Co_2AlO_4/carbon nanofibers @ Co_2AlO_4 nanosheets	after 100 cycles, 810 $mAhg^{-1}$ at 100mAg^{-1} after 400 cycles, 688.5 $mAhg^{-1}$ at 500mAg^{-1}	This work

References:

1 Sara Abouali, Mohammad Akbari Garakani, Biao Zhang, Zheng-Long Xu, Elham Kamali Heidari, Jian-qiu Huang, Jiaqiang Huang, and Jang-Kyo Kim. *ACS Appl. Mater. Interfaces*, 2015, **7**, 13503−13511.

2 Qinxing Xie, Yufeng Zhang, Yating Zhu, Weigui Fu, Xu Zhang, Peng Zhao, Shihua Wu, *Electrochimica Acta*, 2017, **247**, 125–131

3 C. Zhu, X. Mu, P. A. van Aken, Y. Yu and J. Maier, *Angew. Chem. Int. Ed. Engl.*, 2014, **53**, 2152–6.

4 J. Liang, C. Yuan, H. Li, K. Fan, Z. Wei, H. Sun and J. Ma, *Nanomicro. Lett.*, 2018, **10**, 21.

5 M. Zhu, Z. Luo, A. Pan, H. Yang, T. Zhu, S. Liang and G. Cao, *Chem. Eng. J.*, 2018, **334**, 2190–2200.

6 Y. E. Miao, Y. Huang, L. Zhang, W. Fan, F. Lai and T. Liu, *Nanoscale*, 2015, **7**, 11093–101.

7 X. Xie, Y. Hu, G. Fang, X. Cao, B. Yin, Y.Wang, S. Liang, G. Cao and A. Pan, *J. Mater. Chem. A*, 2019, **7**, 16541–16552.